Applied Catalysis B: Environmental 307 (2022) 121137

Contents lists available at ScienceDirect

Applied Catalysis B: Environmental

journal homepage: www.elsevier.com/locate/apcatb

Catalytic hydrogenation of aromatic ring over ruthenium nanoparticles supported on α-Al_2O_3 at room temperature

Wei Jiang [a], Jing-Pei Cao [a,b,*], Chen Zhu [a], Ming Zhao [a], Zhong-Hai Ni [a], Xiao-Yan Zhao [a], Jin-Xuan Xie [a], Liang Zhao [a], Yun-Peng Zhao [a], Hong-Cun Bai [b]

[a] Jiangsu Province Engineering Research Center of Fine Utilization of Carbon Resources, China University of Mining & Technology, Xuzhou 221116, Jiangsu, China
[b] State Key Laboratory of High-Efficient Utilization of Coal and Green Chemical Engineering, Ningxia University, Yinchuan 750021, Ningxia, China

ARTICLE INFO

Keywords:
Aromatic ring hydrogenation
Ruthenium
Al_2O_3
Lignin-derived compounds
Diphenyl ether

ABSTRACT

Selective hydrogenation of aromatic ring represents an essential process for the valorization of lignin in the chemical industry but achieving this process at low temperature is still a challenge. Herein, a series of Ru-based catalysts were investigated. It is found that Ru/γ-Al_2O_3 with small Ru metal particle size shows the low activity in this system. A unique and strong metal-support interaction for Ru/γ-Al_2O_3 indicates that the strongly bounded Ru-O-Al sites lead to the positive charge of Ru species. In contrast, Ru/α-Al_2O_3 with well-dispersed Ru nanoparticles supported on α-Al_2O_3 can successfully catalyze the selective hydrogenation of lignin-derived aromatic compounds at room temperature. Ru/α-Al_2O_3 has the excellent recyclability, air stability and the highest activity. The selective hydrogenation of aromatic ring for Ru/α-Al_2O_3 results from the fast dissociation of H_2 and the high adsorption energy of aromatic ring as revealed by X-ray absorption spectra, X-ray photoelectron spectroscopy and density functional theory calculations.

1. Introduction

Continuous concern on the change of global climate and the depletion of fossil fuels currently leads to tremendous interests on the production of biofuels and chemicals from renewable sources [1,2]. Due to its abundant natural phenolic biopolymer, lignin has the potential to replace crude oil or coal as the source of arenes in prospective chemical industries [3–6]. In addition, the conversion of lignin and its derivatives to biofuels and chemicals makes a significant contribution to a sustainable future [7–9]. The depolymerization of lignin generates many highly oxidized aromatic monomers [10,11]. Most researches are focusing on the cleavage of C-O bonds to transform lignin-derived fragments to arenes, phenols or alcohols, such as catalytic hydrogenolysis [12–15], hydrolysis [16], hydrodeoxygenation [17,18] and so on. In this respect, homogeneous and heterogeneous Ni-based [19–21], Pd-based [22], Ru-based [23,24] and Pt-based [25] catalysts are in rapid development for the reductive cleavage of C-O bonds.

In addition to these general processes, it is urgent to achieve alternative courses based on the selective hydrogenation of aromatic ring for the effective utilization of lignin-derived compounds [10,26–28]. The selective hydrogenation of aromatic ring process will be a new synthesis strategy if it can be realized and controlled. Especially, the selective hydrogenation of aromatic ring can be carried out to synthesize complex compounds. However, it is scarce of the researches on developing highly active and selective catalysts for the aromatic ring hydrogenation. Therefore, the present work aims to meet this need.

Although transition metals, such as Ni and Co, are cheap and widely available, their relatively low activity limits their application for the selective hydrogenation of aromatic ring. The performance of these catalysts in the cleavage of C-O bonds in lignin-derived compounds is excellent. Therefore, they are more suitable for the hydrogenolysis or hydrodeoxygenation processes than for the hydrogenation of aromatic ring [29–31]. In contrast, catalysts containing noble metals are developed rapidly for the hydrogenation of aromatic ring due to their high activity and selectivity. When compared with other noble metal catalysts, such as Pd, Pt and Rh, the lower price of heterogeneous Ru-based catalysts facilitates their wide utilization [32–35]. It is reported that Ru nanoparticles loaded on different types of supports can efficiently catalyze the selective hydrogenation of aromatic ring for lignin-derived compounds under mild conditions [10,36,37]. Cui et al.[10] achieved

* Corresponding author at: Jiangsu Province Engineering Research Center of Fine Utilization of Carbon Resources, China University of Mining & Technology, Xuzhou 221116, Jiangsu, China.
E-mail address: caojingpei@cumt.edu.cn (J.-P. Cao).

https://doi.org/10.1016/j.apcatb.2022.121137
Received 30 September 2021; Received in revised form 14 December 2021; Accepted 21 January 2022
Available online 26 January 2022

Table 1
Effect of the catalyst on the conversion of DPE.

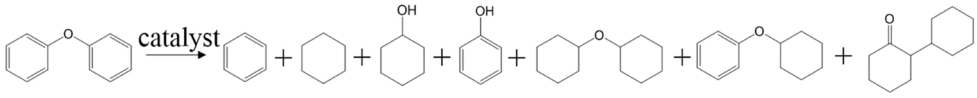

Entry	Catalyst (10% loading)	Con. (%)	Yield (%)						
							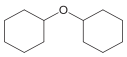	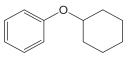	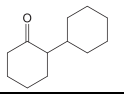
1	None	0	0	0	0	0	0	0	0
2	M	0	0	0	0	0	0	0	0
3	Ru/α-Al_2O_3	100	0	25.3	25.3	0	74.6	0	0.1
4	Ru/γ-Al_2O_3	9.5	0	5.5	5.5	0	0.9	3.1	0
5	Ru/AC	6.2	0	2.6	1.2	1.4	1.5	1.8	0.3
6	Ru/HZSM-5	50.6	0	18.5	15.4	3.1	10.0	17.2	4.9
7	Ru/MgO	57.8	0	15.7	9.3	6.4	14.9	22.5	4.7
8	Ru/ZrO_2	54.5	0	13.8	13.2	0.6	15.8	18.4	6.5
9	Pd/AC	0	0	0	0	0	0	0	0
10	Pd/α-Al_2O_3	0	0	0	0	0	0	0	0

Reaction conditions: 100 mg DPE, 30 mg catalyst, 20 mL isopropanol, 30 °C, 1 MPa H_2, 2 h. M= α-Al_2O_3, γ-Al_2O_3, HZSM-5, MgO, ZrO_2, AC.

Table 2
Effect of the catalyst on the conversion of PHE.

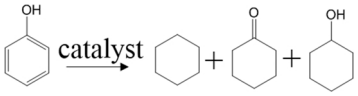

Entry	Catalyst (10% loading)	Con. (%)	Yield/%		
					
1	None	0	0	0	0
2	M	0	0	0	0
3	Ru/α-Al_2O_3	100	0	0	100
4	Ru/γ-Al_2O_3	18.7	0.7	0	18.0
5	Ru/AC	15.2	0	1.4	13.8
6	Ru/HZSM-5	30.0	2.4	2.7	24.9
7	Ru/MgO	40.1	0	3.3	36.8
8	Ru/ZrO_2	38.3	1.9	3.8	32.6
9	Pd/AC	0	0	0	0
10	Pd/α-Al_2O_3	0	0	0	0

Reaction conditions: 100 mg DPE, 30 mg catalyst, 20 mL isopropanol, 30 °C, 1 MPa H_2, 2 h. M= α-Al_2O_3, γ-Al_2O_3, HZSM-5, MgO, ZrO_2, AC.

the hydrogenation of aromatic ring for the lignin-derived compounds at 60–100 °C with Ru-based nanoparticles immobilized on a *N*-doped carbon support. Generally, both the morphology of Ru particles and the metal-support interaction can significantly affect the catalytic performance of monometallic nanocatalysts [36,37]. Wise selection of the support is critical for the selective hydrogenation of aromatic ring under mild conditions [38–40]. Previous studies indicate that the support with a relatively high specific surface area can promote the dispersion of metals to achieve active metals with a relatively small particle size to improve the activity. However, it is found that a high specific surface area and a small metal particle size cannot improve the performance of catalysts in the hydrogenation reaction, especially at a relatively low temperature. Therefore, the metal-support interaction becomes the key factor to control the activity of hydrogenation.

The low bonding energy of active metals can promote the formation of active hydrogen radicals to facilitate the hydrogenation of aromatic ring [41]. The activity of hydrogenation reactions for metals with a positive charge is low because of their low capabilities of both hydrogen dissociation and substrate adsorption. The utilization of metal oxides instead of N- or P- doped carbon as the support can achieve a specific metal-support interaction for some hydrogenation reactions. For instance, Kang et al. [42] reported that synthesized Ru/SiO_2 can effectively catalyze the hydrogenation of benzene (BEN) to cyclohexane (CHN) at 100 °C and 2 MPa H_2. In addition, Ru/γ-Al_2O_3 nanocatalyst is reported to selectively hydrogenate phenol (PHE) under a mild

Table 3
Comparison of the activity of different catalysts.

Entry	Catalyst (10% loading)	DPE Con. (%)	PHE Con. (%)	DPE Time (min)	PHE Time (min)	Rate (mmol $g_{cat.}^{-1}$ h^{-1})		TOF (h^{-1})[a]	
						DPE	PHE	DPE	PHE
1	None	0	0	120	120	0	0	0	0
2	M	0	0	120	120	0	0	0	0
3	Ru/α-Al_2O_3	13.7	10.8	5	5	32.2	58.2	986.0	1405.9
4	Ru/γ-Al_2O_3	9.5	18.7	120	120	0.9	3.3	7.2	25.7
5	Ru/AC	6.2	15.2	120	120	0.6	2.7	1.4	6.1
6	Ru/HZSM-5	8.3	9.7	20	30	4.9	6.9	328.5	463.0
7	Ru/MgO	10.1	12.4	20	30	5.9	8.8	249.9	369.9
8	Ru/ZrO_2	8.9	11.6	20	30	5.2	8.2	377.5	593.2
9	Pd/AC	0	0	120	120	0	0	0	0
10	Pd/α-Al_2O_3	0	0	120	120	0	0	0	0

Reaction conditions: 100 mg DPE or PHE, 30 mg catalyst, 20 mL isopropanol, 30 °C, 1 MPa H_2. M= α-Al_2O_3, γ-Al_2O_3, HZSM-5, MgO, ZrO_2, AC.

[a] The TOFs (mol/($mol_{metal\ Surf.}$ h) = h^{-1}) were normalized by the fractions of accessible Ru atoms on the surface, which were measured by CO chemisorption. The Ru dispersions for Ru/α-Al_2O_3, Ru/γ-Al_2O_3, Ru/AC, Ru/HZSM-5, Ru/MgO and Ru/ZrO_2 were 0.033, 0.130, 0.446, 0.015, 0.024 and 0.014 respectively. The reaction conditions were chosen to allow the determination of the rate below 20% conversion.

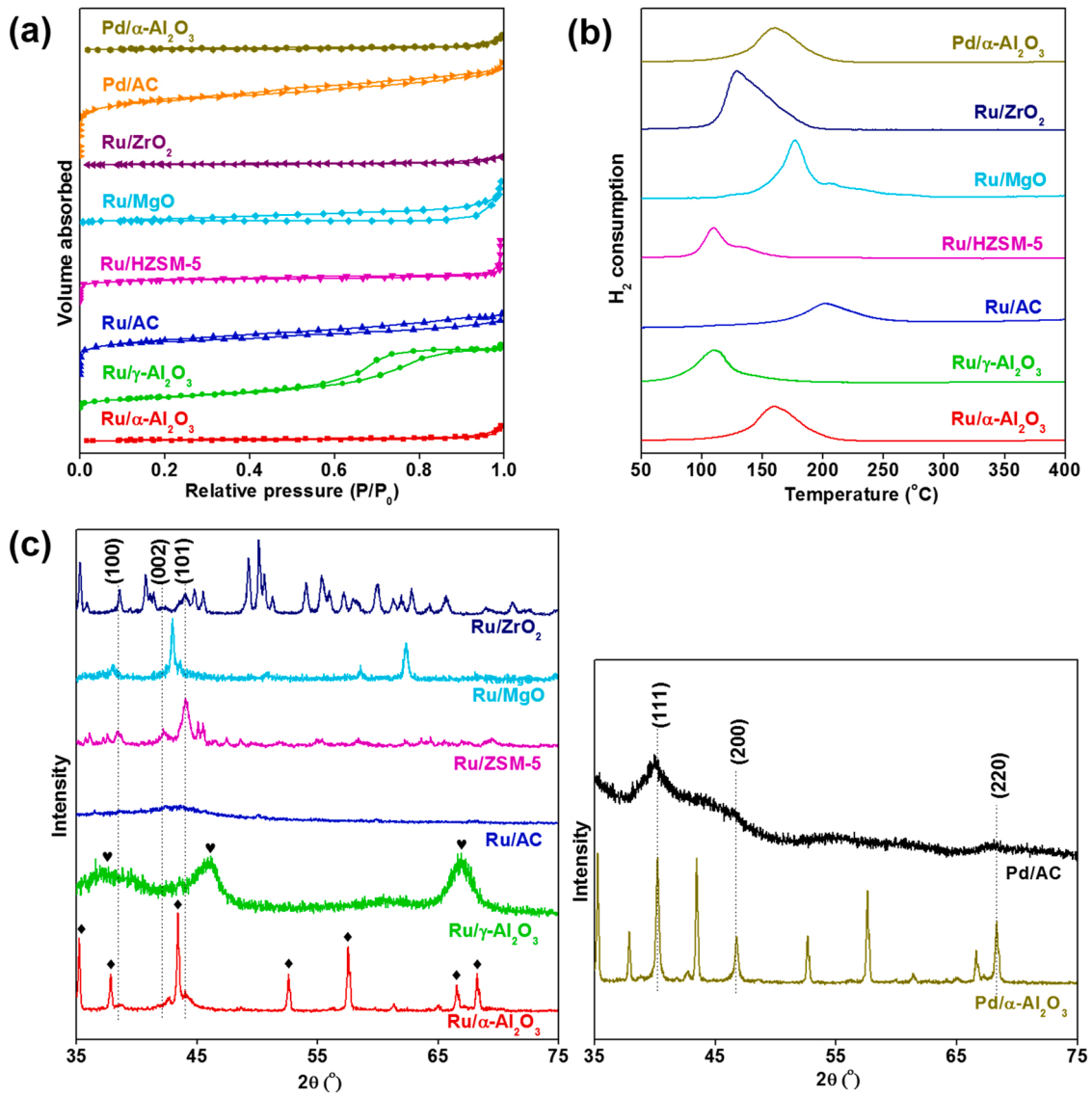

Fig. 1. (a) N_2 adsorption-desorption isotherms, (b) H_2-TPR profile and (c) XRD patterns of different catalysts (10% loading).

condition of 80 °C and 2 MPa H_2 [43]. A Ru catalyst supported on γ-Al_2O_3 is also found to be very active for the hydrogenation of fused aromatic rings, for example, 9-ethylcarbazole, for the application in hydrogen storage [44,45]. The oxide supports, such as alumina, generally have better performance than activated carbon for this type of hydrogenation reaction [38,46]. Although the catalytic hydrogenation of simple alkyl aromatic hydrocarbons, especially BEN and toluene, has been developed rapidly over transition metals including bimetallic catalysts, the heterogeneous catalysts for the hydrogenation of highly functionalized aromatic hydrocarbons and fused-ring aromatics are rather limited [47–49]. Thus, there is a need to design the catalyst to tolerate the functional groups and to fully hydrogenate the fused-aromatic rings under mild conditions.

The aim of this work is to design a series of Ru- and Pd-based catalysts by a conventional wetness impregnation method to test their catalytic performance in the hydrogenation of aromatic ring. The relationship between the structure and the performance of these catalysts is also revealed with a series of characterization methods. Both the activity and product yield of Ru/α-Al_2O_3 for the hydrogenation of various fused-aromatic rings are high. The selective hydrogenation of aromatic ring in multiple lignin-derived compounds can be achieved over Ru/α-Al_2O_3 at room temperature. However, its activity is extremely low in this reaction although γ-Al_2O_3 with a high specific surface area is widely used as the support [50,51]. Traditional Pd-based catalysts with high catalytic performance, such as Pd/AC and Pd/α-Al_2O_3, do not work for the hydrogenation of aromatic ring [34].

2. Experimental section

2.1. Catalyst preparation and characterizations

Ru-based catalysts were synthesized by an incipient wetness impregnation method. Typically, about 0.228 g of $RuCl_3{\cdot}xH_2O$ was dissolved in deionized water before being stirred for 15 min at room temperature. Then about 1 g M (M=α-Al_2O_3, γ-Al_2O_3, HZSM-5, MgO, ZrO_2 or AC) was added to the aqueous solution under continuous stirring and ultrasound for a period of 15 min to form a mixture, which was deposed in a vacuum box for 24 h. After precipitation, the mixture was dried, calcined and reduced to obtain the Ru-based catalysts, which were labeled as 10% Ru/M. The n% Ru/α-Al_2O_3 (n = 1, 4, 7 and 13) and 10% Pd/α-Al_2O_3 were prepared by the same method. The commercial 10% Pd/AC was used for comparison.

These catalysts were well characterized by N_2 adsorption-desorption isotherm measurements, X-ray diffraction (XRD), H_2-temperature

Table 4
Textural properties of different catalysts.

Catalyst (10% loading)	S_{BET} (m^2/g)[a]	S_{micro} (m^2/g)[b]	S_{meso} (m^2/g)[c]	V_{total} (cm^3/g)[d]	V_{micro} (cm^3/g)[b]	V_{meso} (cm^3/g)[c]	D_{ave} (nm)
Ru/α-Al_2O_3	11	0	11	0.09	0	0.09	34.57
Ru/γ-Al_2O_3	195	0	195	0.41	0	0.41	8.40
Ru/AC	807	613	194	0.58	0.26	0.32	2.91
Ru/HZSM-5	360	327	33	0.39	0.14	0.25	4.43
Ru/MgO	74	0	74	0.26	0	0.26	14.10
Ru/ZrO_2	7	0	7	0.05	0	0.05	29.50
Pd/AC	926	702	224	0.62	0.30	0.32	2.69
Pd/α-Al_2O_3	13	0	13	0.11	0	0.11	32.83

S_{BET}: Total pore area; S_{micro}: Micropore surface area; S_{meso}: Mesopore surface area; V_{total}: Total pore volume; V_{micro}: Micropore volume; V_{meso}: Mesopore pore volume; D_{ave}: Average pore diameter.
[a] Determined by multipoint BET method.
[b] Measured by the t-plot method.
[c] By difference.
[d] Calculated from the absorbed volume of nitrogen for a relative pressure P/P_0 of 0.99.

programmed reduction (H_2-TPR), CO chemisorption, scanning electron microscopy (SEM), transmission electron microscopy (TEM), X-ray photoelectron spectroscopy (XPS) and X-ray absorption spectra (XAS) to reveal the relationship between the structure and the activity of the catalyst. The detailed materials, catalyst preparation and characterization methods were listed in the Supporting Information.

2.2. Catalytic reaction

The reaction was carried out in a 100 mL stainless steel autoclave. In a typical experiment, about 100 mg reactant, a certain amount of catalyst (10–50 mg) and 20 mL solvent were put into the reactor. After sealing, the reactor was purged with H_2 for three times before being pressurized to a desired H_2 pressure (0.1–3 MPa) at room temperature. The reaction was performed at room temperature (30 °C) for a certain reaction time (0.5–3 h) with a vigorous stirring speed of 800 rpm. The reaction system decompressed directly during the experiment. The reacted mixture was filtered to remove the catalyst while the obtained organic phase was analyzed by a gas chromatograph-mass spectrometer (GC-MS) and a gas chromatograph (GC). To evaluate the reusability of the catalyst, the mixture was separated by filtration while the solid portion (the catalyst) was carefully washed with isopropanol before being dried at 40 °C under vacuum overnight. Then the catalyst was used directly in the next experiment. The conversion of substrate and the yield of product in the liquid phase were defined by following equations.

$$\text{Conversion} = \frac{\text{moles of substrate reacted}}{\text{total moles of substrate}} \times 100\,(\%) \quad (1)$$

$$\text{Yield} = \frac{\text{moles of product}}{\text{total moles of substrate}} \times 100\,(\%) \quad (2)$$

3. Results and discussion

3.1. Comparison of catalytic performance of different catalysts

The hydrogenation reactions were carried out under mild conditions (30 °C, 1 MPa H_2) with different Ru- and Pd-based nanomaterials as the catalyst. Tables 1 and 2 present the two typical lignin-derived compounds including diphenyl ether (DPE) and PHE, which were selected as the substrates. All the Ru-based catalysts promote the conversion of the two substrates. Ru/α-Al_2O_3 exhibits the highest activity and product yield while Ru/γ-Al_2O_3 displays a relatively low activity and yield. However, both Pd/α-Al_2O_3 and Pd/AC are inactive for the reaction. With DPE as the substrate, the reaction cannot proceed without Ru (Table 1 entries 1–2). Oxydicyclohexane (OCE) is the target product with a relatively high yield of 74.6% when Ru/α-Al_2O_3 is used as the catalyst (Table 1 entry 3). However, the much lower conversion and yield are obtained over other Ru- or Pd-based catalysts (Table 1 entries 4–10). The partial hydrogenation and the cleavage of C-O bonds are two main side reactions to generate cyclohexyl phenyl ether (CPE) and monocycles as the byproduct, respectively. The byproduct of CPE and monocycle aromatic cannot be observed with Ru/α-Al_2O_3 as the catalyst, which indicates the high hydrogenation capability of Ru/α-Al_2O_3 (Table 1 entry 3). For the hydrogenation of PHE, only Ru/α-Al_2O_3 can achieve a full conversion of the substrate to generate a single product of cyclohexanol (CHL) (Table 2 entry 3). Other Ru- or Pd-based catalysts show much lower activity than Ru/α-Al_2O_3 (Table 2 entries 4–10). Cyclohexanone can be detected when Ru/MgO, Ru/ZrO_2, Ru/HZSM-5 and Ru/AC are used as the catalysts, which suggests their weak hydrogenation performance (Table 2 entries 5–8). This result is consistent with the hydrogenation of DPE.

As shown in Table 3, both the reported reaction rates and turnover frequencies (TOFs) correspond to the initial conversion. Determined from the low conversion, the initial rates of the hydrogenation of DPE and PHE over Ru/α-Al_2O_3 are 32.2 and 58.2 mmol $g_{cat.}^{-1}$ h^{-1}, respectively (Table 3 entry 3). If the rates are normalized to per mole of surface Ru atoms, TOFs of individual reactions for the hydrogenation of DPE and PHE over Ru/α-Al_2O_3 are 986.0 and 1405.9 h^{-1}, respectively (Table 3 entry 3). As excepted, Ru in Ru/α-Al_2O_3 shows the highest rate and TOF than Ru in other Ru- or Pd-based catalysts under similar conditions for the hydrogenation of DPE and PHE, indicating the highest activity of Ru/α-Al_2O_3.

3.2. Catalyst characterization

Fig. 1a shows that the N_2 adsorption-desorption isotherms vary with the type of Ru- and Pd-based catalysts, which indicates that different number of micropores or mesopores are distributed in these catalysts. As listed in Table 4, Ru/AC, Pd/AC and Ru/HZSM-5 catalysts contain a large number of micropores and a small number of mesopores, while only a small number of mesopores are present in the other catalysts. Among these catalyst supports, traditional activated carbon has the largest total specific surface area, the largest total pore volume and the smallest average pore diameter due to its highly developed pore structure. Generally, the support with a large specific surface area facilitates the distribution of active metal particles and the catalyst with highly distributed active sites significantly improves the catalytic performance and reaction efficiency. Notably, the total specific surface area of Ru/α-Al_2O_3 is smaller than that of Ru/γ-Al_2O_3. Pd/α-Al_2O_3 and Ru/α-Al_2O_3 have the same catalyst support and similar pore structure characteristic.

As shown in Fig. 1b, the current reduction peaks are ascribed to the reduction processes of RuO_2 and PdO to elemental Ru and Pd, respectively. The reduction temperature of these catalysts was selected as 300 °C. The XRD patterns of the reduced Ru- and Pd-based catalysts are displayed in Fig. 1c. According to ICSD 60,419 (PDF 01-077-2135), typical diffraction peaks at 2θ of 35.14°, 37.78°, 43.36°, 52.55°, 57.52°, 66.55° and 68.20° are assigned to (104), (110), (113), (024), (116), (214) and (300), respectively. This confirms that the Al_2O_3 support is α-phase. The diffraction lines at 2θ of 37.60°, 45.79° and 66.76° are ascribed to the lattice planes of (311), (400) and (440), respectively. This suggests that the Al_2O_3 support is γ-phase, which is consistent with the result in the literature [52]. Compared with the γ-Al_2O_3 phase, the XRD pattern demonstrates that the peak of the α-Al_2O_3 phase is more intense, revealing the perfect formation of crystalline [53]. For the series of Ru-based catalysts, main diffraction peaks can be observed at 2θ of 38.38°, 42.18° and 44.01°, which corresponds to the elemental Ru planes of (100), (002) and (101), respectively [54,55]. For Pd/α-Al_2O_3

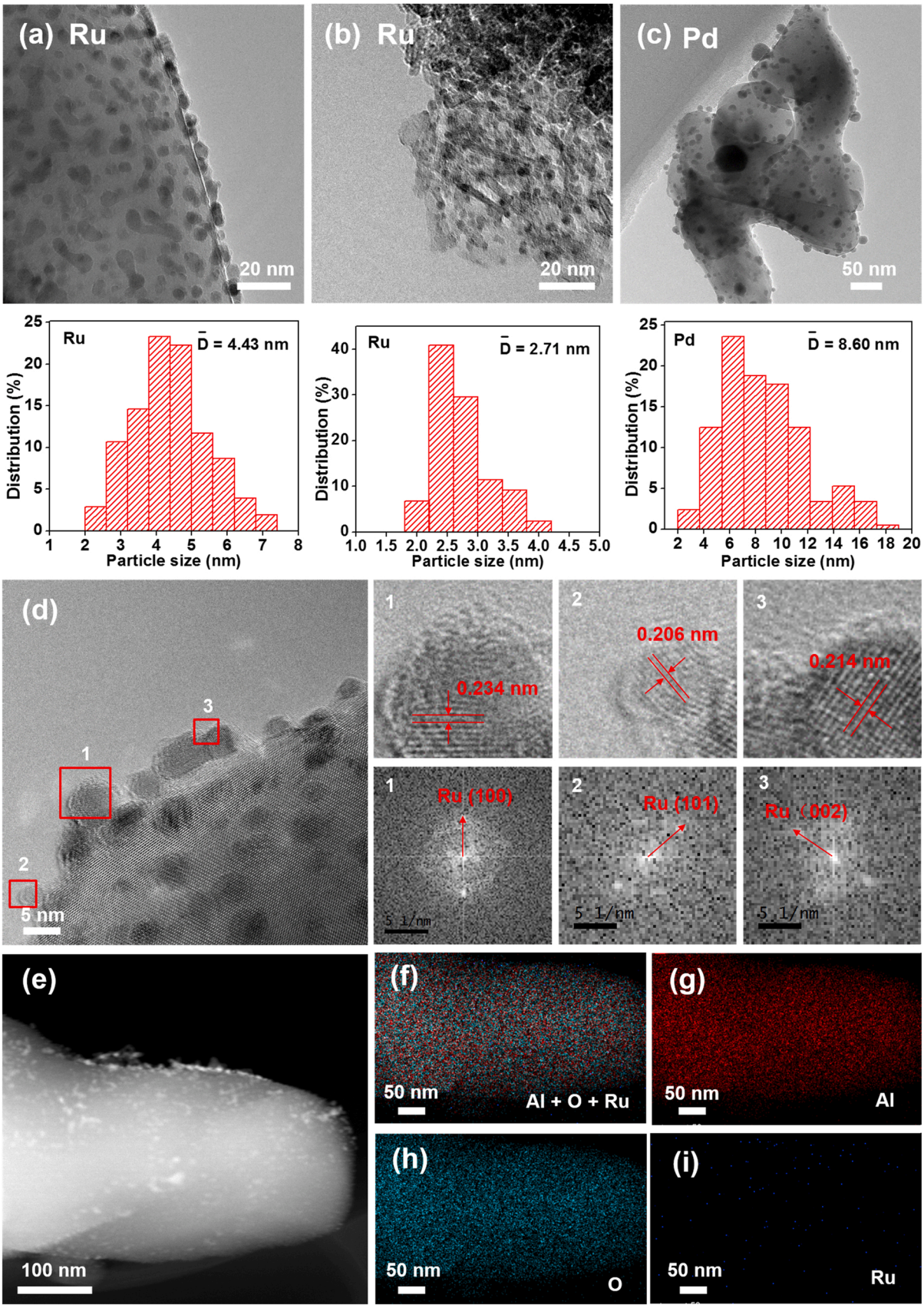

Fig. 2. TEM images and the histograms of the metal size distributions of reduced (a) Ru/α-Al_2O_3, (b) Ru/γ-Al_2O_3 and (c) Pd/α-Al_2O_3 before reaction, (d) HRTEM image, lattice and SAED pattern of Ru in the reduced Ru/α-Al_2O_3, (e) HAADF-STEM image and (f-i) HAADF-STEM elemental mappings of the reduced Ru/α-Al_2O_3 (10% loading).

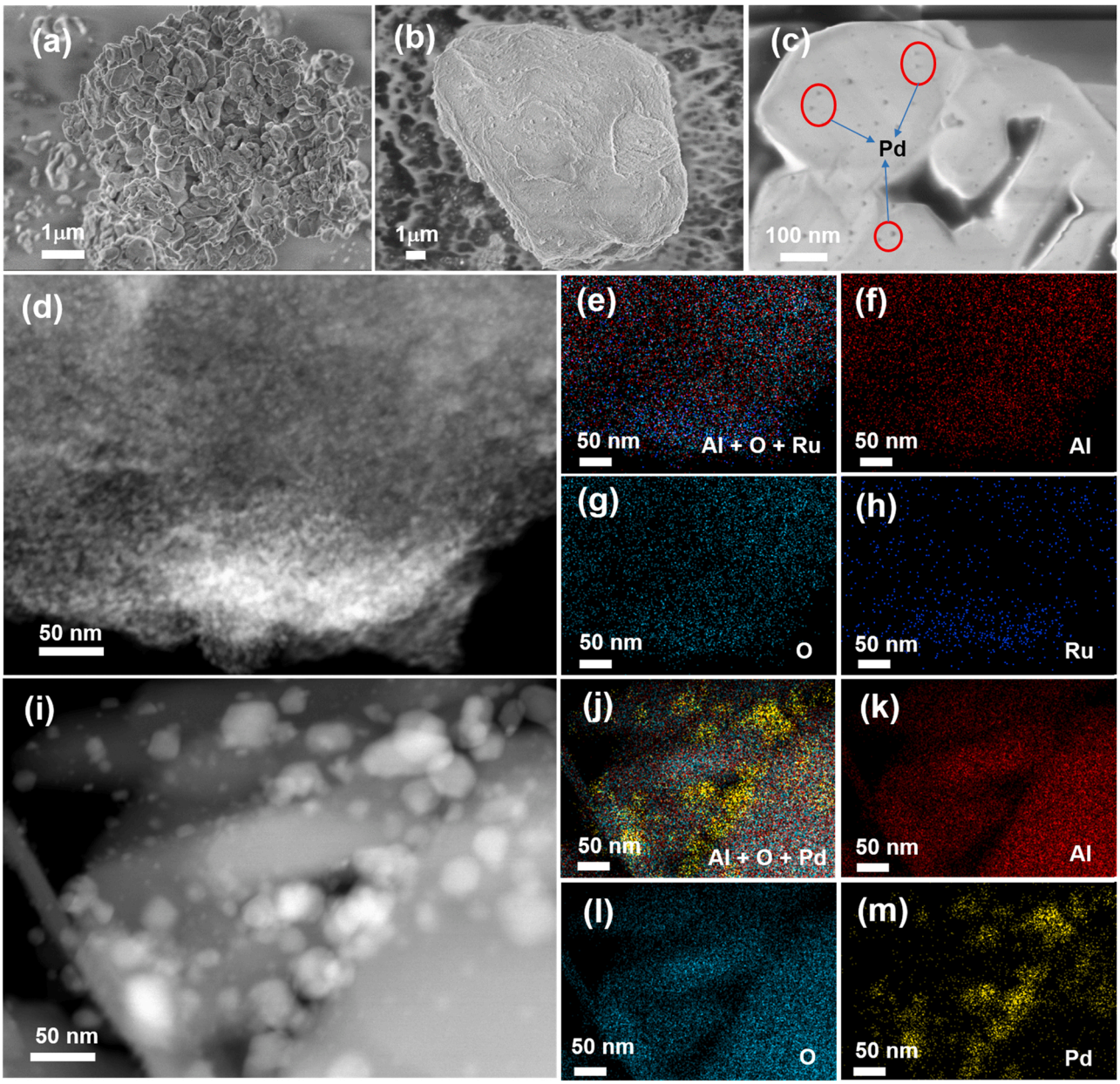

Fig. 3. SEM images of the reduced (a) Ru/α-Al_2O_3, (b) Ru/γ-Al_2O_3 and (c) Pd/α-Al_2O_3; (d) HAADF-STEM image and (e-h) HAADF-STEM elemental mappings of the reduced Ru/γ-Al_2O_3; (i) HAADF-STEM image and (j-m) HAADF-STEM elemental mappings of the reduced Pd/α-Al_2O_3 (10% loading).

and Pd/AC, three diffraction peaks appearing at 2θ of 40.14°, 46.69° and 68.17°, are attributed to (111), (200) and (220) planes of elemental Pd, respectively. The diffraction peak intensity of Pd/AC is weaker than that of Pd/α-Al_2O_3, indicating the higher dispersion of elemental Pd on AC, as suggested by other studies [56,57]. The peak intensity of the Ru-based catalysts is slighter than that of the Pd-based catalysts. Especially for the catalysts with the same support of α-Al_2O_3, the diffraction peaks of metal Ru for Ru/α-Al_2O_3 are hard to be detected with XRD while the peaks of metal Pd are strong in Pd/α-Al_2O_3.

In order to better analyze the dispersion of metals in the catalysts, the catalysts of Ru/α-Al_2O_3, Ru/γ-Al_2O_3 and Pd/α-Al_2O_3 are characterized as typical representatives. As shown in Fig. 2, the TEM images indicate that the average particle size of Ru in Ru/α-Al_2O_3 and Ru/γ-Al_2O_3 is around 4.43 and 2.71 nm, respectively, without any agglomeration. However, the average size of Pd in Pd/α-Al_2O_3 is about 8.60 nm with a certain degree of agglomeration. The result implies that elemental Ru forms relatively small particles dispersed on α-Al_2O_3 and γ-Al_2O_3, which results in the weak signals of the XRD diffraction peaks for Ru [52]. The particle size of Pd is much larger than that of Ru although the two catalysts are synthesized with the same method. It suggests that for the same catalyst support and the same type of precursor, the Pd particles are larger than of the Ru particles. This indicates that Pd has a higher tendency to agglomerate and to obtain a large particle size than Ru, which is consistent with other works [58,59].

The particle size of metal Ru in Ru/γ-Al_2O_3 is significantly smaller than that in Ru/α-Al_2O_3 because a high specific surface area of the support promotes the dispersion of the metal. As presented in Fig. 2d, the bright spots observed in the corresponding selected area electron diffraction (SAED) patterns can be indexed to different planes of Ru in Ru/α-Al_2O_3 by using the comparative *d* spacings method, which suggests that the Ru nanoparticles are single crystal. The palpable crystal lattices with an interplanar distance of 0.234, 0.206 and 0.214 nm correspond well to (100), (101) and (002) planes of Ru, respectively, which is highly consistent with the result of XRD analysis. The SEM images (Figs. 3a, 3b,

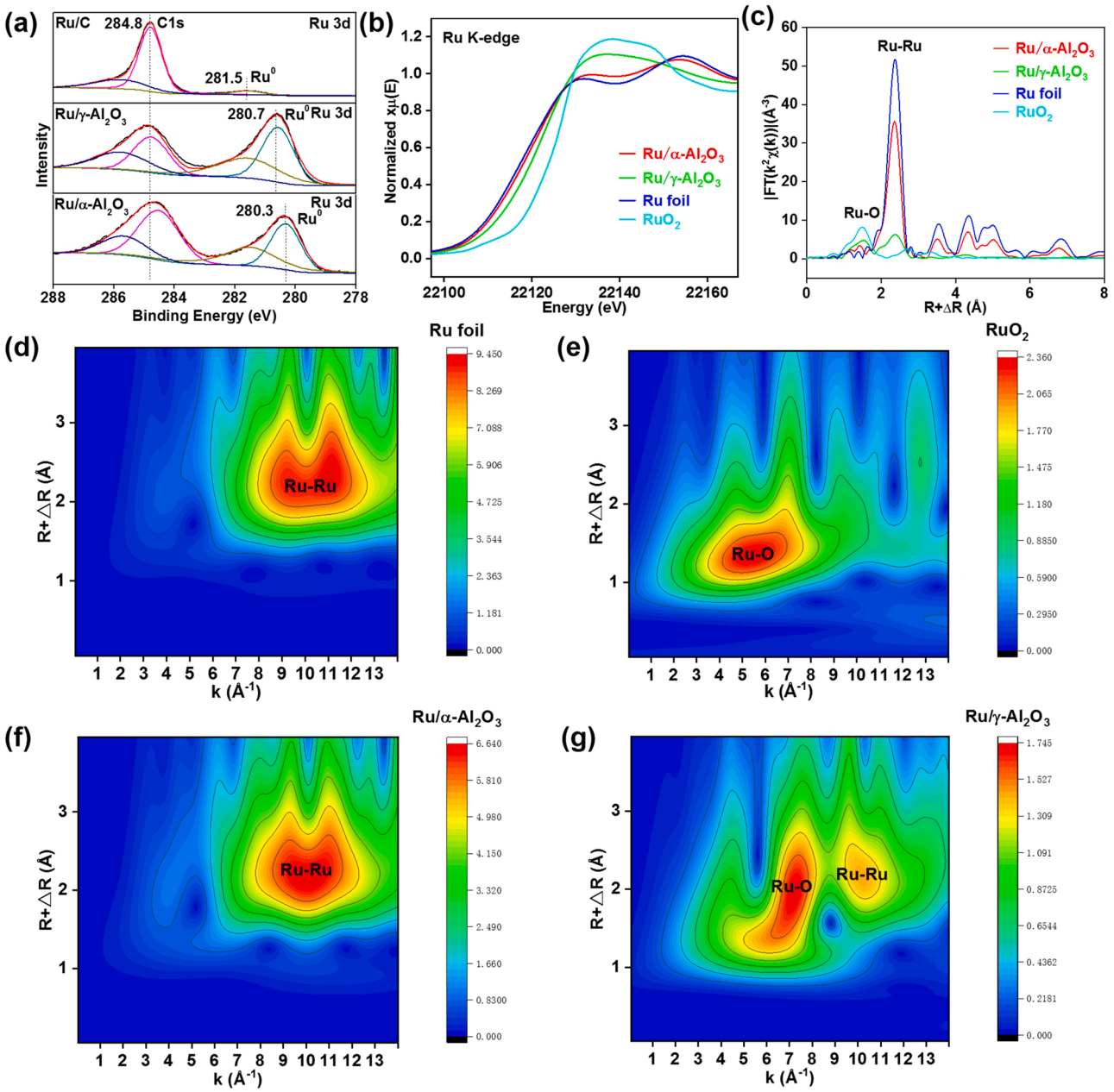

Fig. 4. (a) The XPS spectra of Ru 3d in Ru/C, Ru/α-Al_2O_3 and Ru/γ-Al_2O_3, (b) XANES spectra for Ru K-edge, (c) Fourier transformed (FT) k^2-weighted χ(k)-function of EXAFS spectra for Ru K-edge, (d-g) The wavelet transforms for the k^2-weighted Ru K-edge EXAFS signals of Ru foil, RuO_2, Ru/α-Al_2O_3 and Ru/γ-Al_2O_3 (10% loading).

Table 5
EXAFS fitting parameters at the Ru K-edge for different samples (S_0^2 =0.80).

Samples	shell	[a]CN	[b]R (Å)	[c]σ^2	[d]ΔE_0	R factor
Ru foil	Ru-Ru	12	2.68 ± 0.01	0.0039	-0.1 ± 0.8	0.0136
RuO_2	Ru-O	5.9 ± 0.1	1.98 ± 0.01	0.0058	-1.9 ± 0.6	0.0129
	Ru-Ru	4.6 ± 0.8	3.20 ± 0.01	0.0124		
Ru/α-Al_2O_3	Ru-Ru	10.0 ± 0.9	2.68 ± 0.01	0.0047	-4.6 ± 0.9	0.0192
Ru/γ-Al_2O_3	Ru-Ru	3.3 ± 0.3	2.68 ± 0.03	0.0066	-3.3 ± 1.4	0.0214
	Ru-O	3.2 ± 0.3	1.97 ± 0.02	0.0061		

[a] *CN*: coordination numbers.
[b] *R*: bond distance.
[c] σ^2: Debye-Waller factors.
[d] ΔE_0: the inner potential correction; *R* factor: goodness of fit. S_0^2 was set to 0.80, according to the experimental EXAFS fit of Ru foil reference by fixing CN as the known crystallographic value; δ: percentage.

Table 6
Effect of solvent on the conversion of DPE over 10% Ru/α-Al_2O_3.

Entry	Solvent	Con. (%)	Yield (%)						
							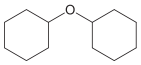	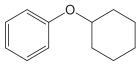	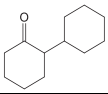
1	*n*-Hexane	99.8	0	24.2	24.2	0	70.9	1.6	3.1
2	Tridecane	53.1	0	7.7	7.7	0	29.7	5.6	10.1
3	Methanol	99.5	0	43.9	43.9	0	40.4	4.6	10.6
4	Ethanol	82.7	0	29.6	29.6	0	24.3	18.9	9.9
5	*n*-Butanol	40.1	0	7.1	7.1	0	9.1	19.1	4.8
6	Isopropanol	100	0	25.3	25.3	0	74.6	0	0.1

Reaction conditions: 100 mg DPE, 30 mg catalyst, 20 mL solvent, 30 °C, 1 MPa H_2, 2 h.

3c) show that the metal Ru cannot be observed on the surface of α-Al_2O_3 and γ-Al_2O_3 due to its perfect dispersion and smaller particle size, while Pd can be clearly observed on the surface of α-Al_2O_3 because of its larger particle size. The HAADF-STEM image and HAADF-STEM elemental mappings of Ru/α-Al_2O_3 (Fig. 2e-i) and Ru/γ-Al_2O_3 (Fig. 3d-h) demonstrate that the Ru metal is dispersed evenly on the surface of the supports without any agglomeration. However, the metal Pd in Pd/α-Al_2O_3 (Fig. 3i-m) presents obvious agglomeration on the surface of the support.

According to the above results, Ru/α-Al_2O_3 has a much smaller total specific surface area and a larger particle size of metal Ru than Ru/γ-Al_2O_3, but the catalytic activity and product yield of Ru/α-Al_2O_3 are significantly higher than that of Ru/γ-Al_2O_3 and especially that of Ru/AC. In addition, both Pd/α-Al_2O_3 and Pd/AC are almost inactive. It was reported that the Pd-based catalysts are usually considered as poor catalysts for the hydrogenation of most aromatic rings at relatively low temperatures, and the reaction conditions are often harsh, for example, in supercritical CO_2 fluids under a high pressure [60,61]. The results demonstrate that the specific surface area and the metal particle size distribution of the catalyst are not the main factors for the selective hydrogenation of aromatic ring at the relatively low reaction temperature in the present study.

To accurately explore the local atomic and electronic structure of the Ru-based catalysts, XPS, extended X-ray absorption fine structure (EXAFS) and X-ray absorption near edge structure (XANES) measurements were employed. As shown in Fig. 4a, the binding energy was corrected with the C 1s binding energy determined at 284.8 eV. Since the peak of Ru $3d_{3/2}$ is overlapped with the peak of C 1s, the Ru $3d_{3/2}$ peak cannot be observed. The Ru $3d_{5/2}$ peaks at 280.3, 280.7 and 281.5 eV are attributed to Ru^0 in Ru/α-Al_2O_3, Ru/γ-Al_2O_3 and Ru/AC, respectively. Due to the difference in the size of metal Ru, it cannot be directly considered that the shift of the Ru^0 bonding energy is caused by the change in the valence state of Ru. Therefore, a catalyst with a low Ru loading (5% Ru/α-Al_2O_3) was prepared for comparison. As shown in Fig. S2, the average particle size of Ru in 5% Ru/α-Al_2O_3 catalyst can be reduced to 2.1 nm. No obvious shift of the Ru^0 bonding energy can be observed for Ru/α-Al_2O_3 with a content of Ru between 5% and 10% (Fig. S3), which proves that the shift of the Ru^0 bond energy is mainly attributed to the difference in the Ru valence states for different catalysts. A lower binding energy of Ru^0 in Ru/α-Al_2O_3 indicates that α-Al_2O_3 leads to the display of the high electron density of Ru, which facilitates the rapid dissociation of H_2, as suggested by other studies [41,54].

The XANES spectra of Ru K-edge as shown in Fig. 4b suggests that the energy absorption threshold of Ru/α-Al_2O_3 and Ru/γ-Al_2O_3 is between that of Ru foil and RuO_2. The Ru K-edge of Ru/α-Al_2O_3 is closer to Ru foil than that of Ru/γ-Al_2O_3. This suggests the low bonding energy of Ru/α-Al_2O_3 while the positive charge of Ru species in Ru/γ-Al_2O_3, which is in good agreement with the XPS result [62]. The EXAFS analysis also reveals the same trend. As shown in Fig. 4c, Ru/α-Al_2O_3 has a stronger peak of Ru-Ru while a weaker peak of Ru-O than Ru/γ-Al_2O_3. The EXAFS wavelet transforms (WT) analysis (Fig. 4d-g) not only provides the radial distance resolution but also the k-space resolution to further identify the atomic Ru dispersion. The Ru foil benchmark shows a maximum intensity at 10 $Å^{-1}$ while the RuO_2 displays a maximum intensity at 6 $Å^{-1}$, which are ascribed to the Ru-Ru scattering and the Ru-O scattering, respectively. Both the Ru-Ru scattering and Ru-O scattering can be found for Ru/γ-Al_2O_3, whereas only one maximum intensity at 10 $Å^{-1}$ can be detected for Ru/α-Al_2O_3. This indicates that for Ru/α-Al_2O_3, the Ru is in the form of a mononuclear Ru center in the absence of other Ru species, which is consistent with the works of others [63,64]. No obvious difference can be observed in the corresponding position of the Ru-Ru scattering between the Ru/α-Al_2O_3 catalyst and the Ru foil. Other studies suggest that there are two types of the Ru-O scattering for Ru/γ-Al_2O_3: the Ru-O site, where the surface Ru is oxidized by oxygen in the air, and the interfacial Ru-O-Al bonding formed under strong reducing conditions in Ru/γ-Al_2O_3 [65,66]. However, a significant position difference in the Ru-O scattering can be observed for Ru/γ-Al_2O_3 and RuO_2, indicating that the interfacial Ru-O-Al bonding is mainly responsible for the Ru-O scattering for Ru/γ-Al_2O_3. The strong metal-support interaction of the bounded Ru-O-Al sites in Ru/γ-Al_2O_3 leads to the significant oxidation of metal Ru, which weakens the ability of Ru/γ-Al_2O_3 catalyst to dissociate H_2. In addition, as listed in Table 5, the larger coordination numbers (CN) of Ru-Ru bonds in Ru/α-Al_2O_3 indicates that the particles size of Ru in Ru/α-Al_2O_3 is larger than that in Ru/γ-Al_2O_3, which is consistent with the TEM analysis.

3.3. *Different parameters for the hydrogenation of arene over Ru/α-Al_2O_3*

In order to explore the effect of solvents on the catalytic activity and hydrogen transfer mechanism, the hydrogenation reactions of DPE were carried out with different solvents and atmospheres as listed in Table 6. Generally, hydrogen-donating solvents can directly provide the hydrogen source for the hydrogenation reaction [23]. However, the reaction doesn't proceed for every solvent under the Ar atmosphere, which reveals that the hydrogen source is directly provided by H_2 rather than by the solvents. In addition, the nonspecific (van der Waals) or weak specific (H-bonding) interactions between the substrate and the solvents cannot induce the aromatic ring hydrogenation of DPE, which results from the strong interaction established between the active metal site and the substrate on the surface of the catalyst. However, other studies suggest that the solubility of H_2 varies with the type of the solvent, which influences the rate of H_2 conversion to active hydrogen and causes the different reaction rates [67,68]. For the fast H_2 transfer, such as *n*-hexane, methanol and isopropanol, a high conversion can be observed. The yield of target product is the highest only under isopropanol as the solvent, suggesting the highest activity of isopropanol for the hydrogenation of aromatic ring. The smaller the number of carbons in the linear alkanes used, the higher the catalytic performance can be achieved in this system. Additionally, the activity gradually decreases with an increase in the number of carbons in the linear *n*-alcohols. It can be explained that H_2 cannot be easily converted to hydrogen radicals due to the increasing concentration of the solvent [69].

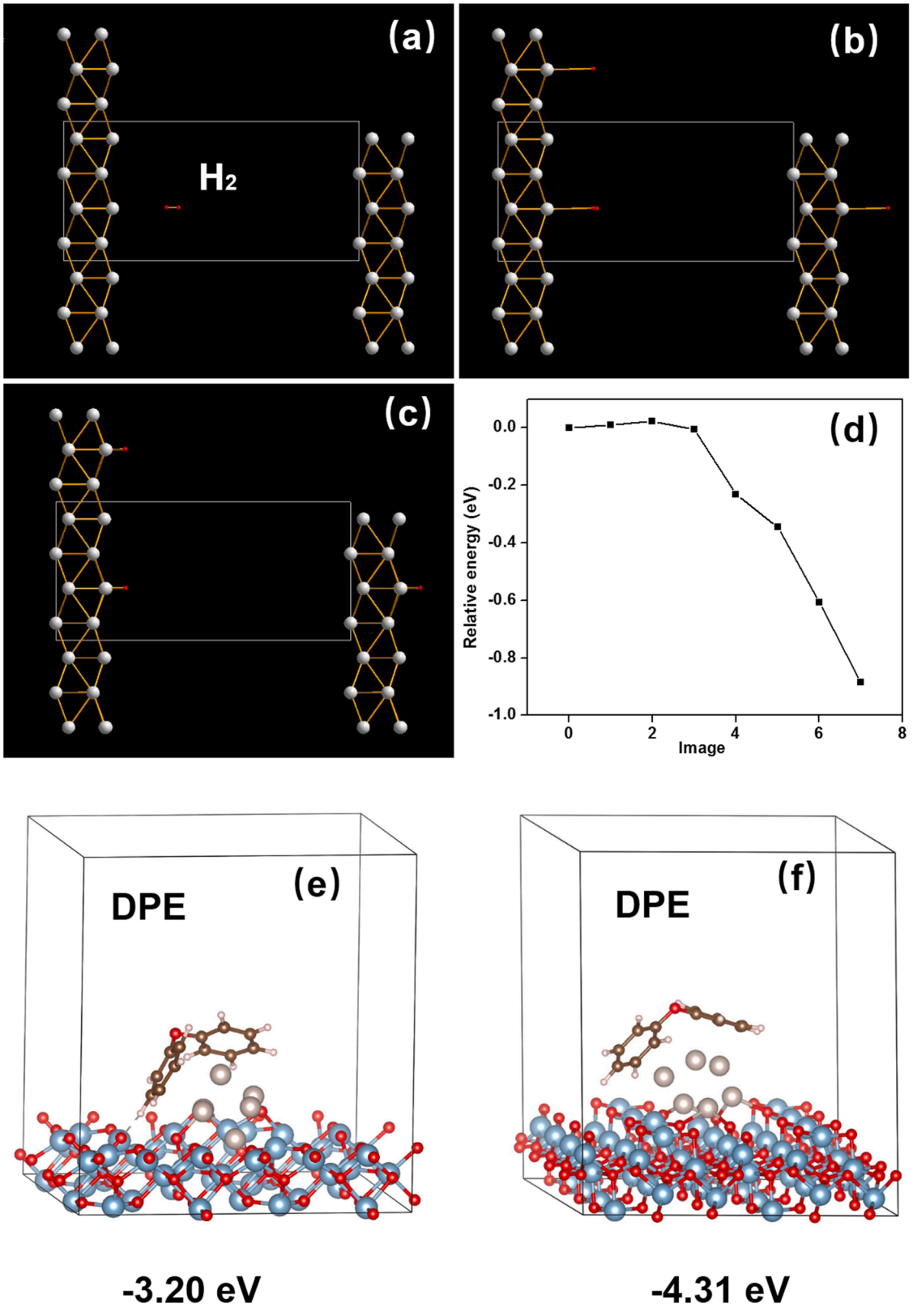

Fig. 5. (a), (b) and (c) The structural diagrams of the pathway for the hydrogen dissociation on Ru (100), (The white balls represent the Ru atoms while the red balls represent the hydrogen atoms), (d) The energy along the CI-NEB pathway. The adsorption geometry and the calculated adsorption energy of DPE over (e) Ru/γ-Al_2O_3 and (f) Ru/α-Al_2O_3.

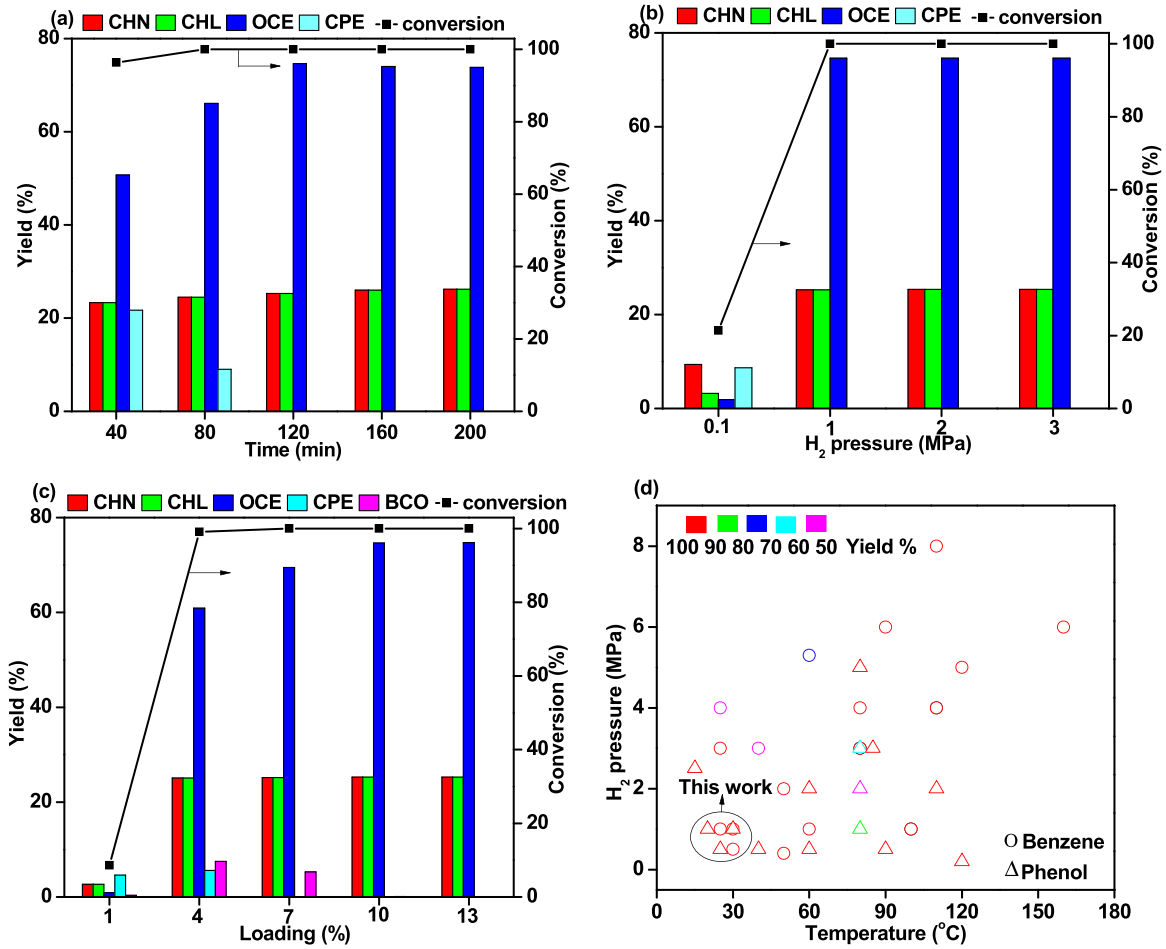

Fig. 6. The effects of (a) reaction time, (b) reaction pressure and (c) catalyst loading on the conversion of DPE, (d) The comparison between the hydrogenation conditions of the present study and of the reported results in the literature (Tables S1 and S2). Reaction conditions: 100 mg DPE, 30 °C, 20 mL isopropanol, (a) 30 mg 10% Ru/α-Al_2O_3, 1 MPa H_2, (b) 30 mg 10% Ru/α-Al_2O_3, 2 h, (c) 30 mg Ru/α-Al_2O_3 catalyst, 1 MPa H_2, 2 h.

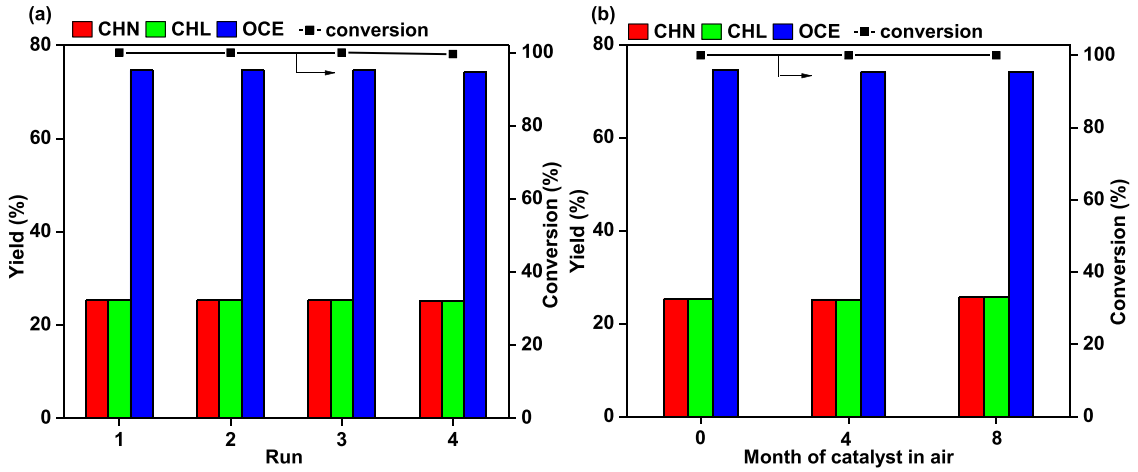

Fig. 7. (a) The recyclability and (b) air stability of 10% Ru/α-Al_2O_3 for the conversion of DPE. Reaction conditions: 100 mg DPE, 30 °C, 30 mg catalyst, 20 mL isopropanol, 1 MPa H_2, 2 h.

Therefore, isopropanol is the best solvent to achieve both high activity and selectivity for the hydrogenation of aromatic ring.

Density functional theory (DFT) calculation was performed using the VASP program (The details can be found in the Supporting Information) to reveal the dissociation and the transfer processes of H_2. As shown in Fig. 5, firstly, H_2 adsorbs on the Ru metal to form H_2 * and the △E of this process is calculated as − 0.6 eV (Eq. 3). Subsequently, − 0.89 eV of △E is calculated for the dissociation of H_2 * into two highly active hydrogen radicals, which immediately combine with the substrate for the hydrogenation of aromatic ring (Eq. 4). Therefore, the barrier for the dissociation of H_2 on Ru is calculated as 0.02 eV. The main reason why the hydrogenation reaction occurs at room temperature is that H_2 can be

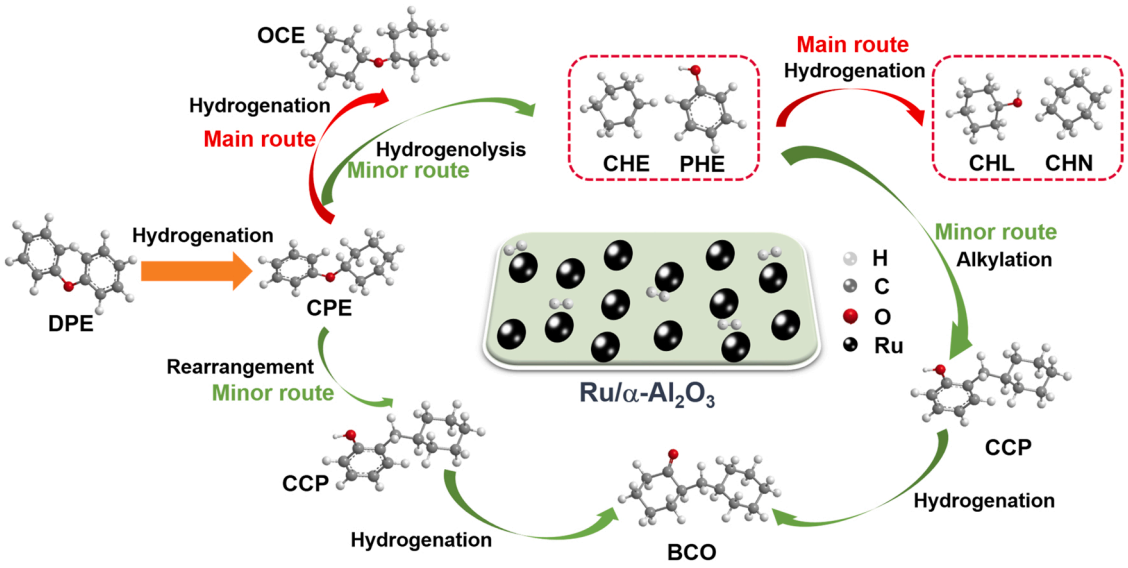

Fig. 8. Reaction pathways for the conversion of DPE over Ru/α-Al_2O_3 catalyst.

easily dissociated into active hydrogen radicals on the surface of metal Ru. In addition, the adsorption energy of DPE for the two catalysts is also calculated with DFT (The details can be found in the Supporting Information). The most stable adsorption mode of DPE was angular. The adsorption energy is calculated to be − 3.20 eV for Ru/γ-Al_2O_3 and − 4.31 eV for Ru/α-Al_2O_3, respectively, which indicates that the adsorption capacity of DPE for Ru/α-Al_2O_3 is stronger.

$$Ru + H_2 \rightarrow H_2^* \ \Delta E = -0{\cdot}60 \text{ eV} \quad (3)$$

$$H_2^* \rightarrow (H{+}H)^* \ \Delta E = -0{\cdot}89 \text{ eV} \quad (4)$$

The kinetics behaviors for the conversion of DPE were conducted over Ru/α-Al_2O_3 by changing several important parameters. As depicted in Fig. 6a, the conversion of DPE is higher than 90% after a reaction time of only 40 min and quickly reaches the maximum value of 100% for a reaction time of 120 min, which implies the high activity of Ru/α-Al_2O_3. With the further increase in the reaction time, the yield of both CHN and CHL increases slightly before reaching a stable value of about 26% while an obvious increase in the yield of OCE and a decrease in the yield of CPE can be observed. This indicates that CPE is mainly converted to OCE rather than to monocycle through the cleavage of C-O bonds. Both CHN and CHL are probably produced by the direct hydrogenolysis of DPE. After a reaction time of 120 min, the major products are CHN, CHL and OCE. A complete conversion of DPE can be achieved in a shorter reaction time than the cases reported in previous studies [10,70], suggesting the higher activity of Ru/α-Al_2O_3.

The effect of the H_2 pressure on the conversion of DPE over Ru/α-Al_2O_3 is presented in Fig. 6b. As mentioned above, there is almost no conversion of DPE in the absence of H_2. At a relatively low H_2 pressure of 0.1 MPa, the activity of Ru/α-Al_2O_3 is very low. The yield of CHN is greater than that of CHL due to the partially unhydrogenated PHE. However, almost no BEN can be detected during the conversion process of DPE. This reveals that PHE is an important intermediate product but BEN is not. At a H_2 pressure of 1 MPa, both the conversion of DPE and the yield of target product reach their maximum value before remaining at stable value. The yield of CHL is similar to that of CHN due to the hydrogenolysis-hydrogenation tandem process. A proper hydrogen pressure is essential for the aromatic ring hydrogenation of DPE. For the case of Ru/α-Al_2O_3, the optimal hydrogen pressure is determined to be about 1 MPa to obtain a full conversion of DPE and a relatively high yield of target product.

The relationship between the product distribution with Ru metal loading (1–13 wt%) was investigated. As shown in Fig. 6c, for a low loading of Ru (1–4 wt%), partially hydrogenated CPE can be detected due to the lack of the active metal site. [1′-bicyclohexyl]− 2-one (BCO) can be found for a medium loading of Ru (4–7 wt%). The literature [71] reveals that the carbon-carbon coupling product of BCO can be obtained by modifying the ratio between the active metal and the acidic site of the catalyst. The yield of BCO reaches the maximum value with a Ru loading of 4 wt% before gradually decreasing with the further increase in the Ru loading until almost no BCO can be found with a Ru loading of 10 wt%. Fig. 7a shows that Ru/α-Al_2O_3 catalyst can be reused for at least four cycles without any reduction in activity. No significant difference can be observed for the fresh and the spent Ru/α-Al_2O_3 catalyst as characterized by both XRD and TEM (Fig. S4 and S5). These results indicate that Ru/α-Al_2O_3 is very stable under the reaction conditions of the present study. Additionally, the activity of Ru/α-Al_2O_3 can be maintained after being placed in air for eight months (Fig. 7b), implying the air stability of Ru/α-Al_2O_3.

3.4. Reaction pathway

Based on the above analysis, the possible reaction mechanism for the conversion of DPE is proposed in Fig. 8. CPE is a partial hydrogenation product of DPE. Both CHL and CHN are probably produced by a hydrogenolysis-hydrogenation process. If both BEN and PHE can be formed during the conversion of DPE, there must be BEN in the system before PHE being completely hydrogenated because other studies suggest that BEN is more difficult to be hydrogenated than PHE [7,72,73]. However, only part of the unhydrogenated PHE can be detected while almost no of BEN can be found in the reaction system. This suggests that the direct hydrogenolysis of both DPE to BEN and PHE cannot be achieved. Therefore, DPE is first hydrogenated to CPE incompletely. Then most of CPE is further hydrogenated to the target product of OCE. Similarly, the direct hydrogenolysis of CPE to produce BEN and CHL cannot be achieved.

A relatively small amount of BCO can also be found during the conversion of DPE. Chen et al. [59] concluded that two PHE can be finally converted to BCO through a condensation reaction or an electrophilic aromatic substitution reaction. However, this process will lead to a significant decrease in the yield of PHE, which results in a higher yield of CHN than that of CHL after the complete hydrogenation. This is not consistent with the experimental result. Therefore, the existence of the partially unhydrogenated PHE suggests that the most possible pathway for the formation of BCO is that CPE goes through a hydrogenolysis reaction to produce PHE and cyclohexene (CHE), which are

Table 7
Selective hydrogenation of arene over 10% Ru/α-Al_2O_3.

Entry	Pressure/MPa	Time/h	Substrate	Product	Yield/Conversion (%)
1	1	2			100/100
2	1	3	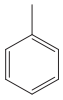	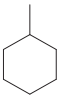	100/100
3	1	3	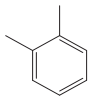	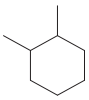	100/100
4	1	3	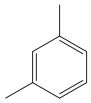	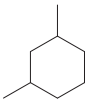	100/100
5	1	3	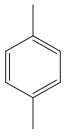	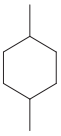	100/100
6	1	2	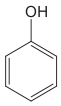	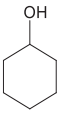	100/100
7	1	2	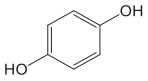	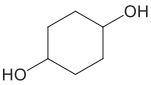	100/100
8	1	2	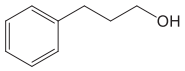	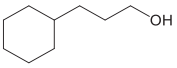	100/100
9	3	2	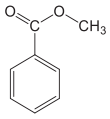	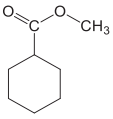	100/100
10	1	2	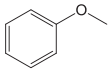	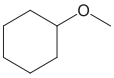	100/100
11	1	2	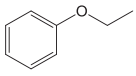	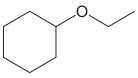	100/100
12	3	24	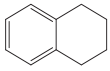	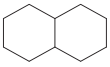	99.6/100
13	3	12	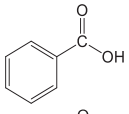	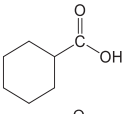	95.5/100
14	1	2	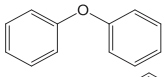	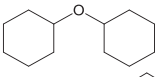	74.6/100
15	1	2	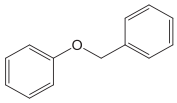	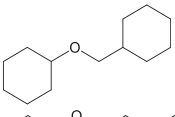	91.9/100
16	1	2	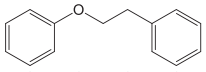	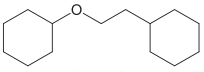	90.6/100
17	1	2	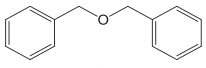	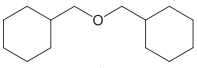	98.5/100
18	1	2	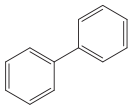	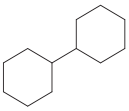	100/100
19	3	24	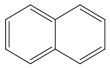	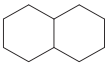	93.8/100

Reaction conditions: 100 mg substrate, 30 mg catalyst, 20 mL isopropanol, 30 °C.

further converted to 2-cyclohexylphenol (CCP) via alkenylation. Finally, CCP is fully hydrogenated to BCO. This result is in good agreement with the literature [71]. However, CHE cannot be detected in the reaction system because its formation rate is relatively low while its conversion rate by the alkylation reaction or by the further hydrogenation to CHN is relatively high. Meanwhile, the conversion of CCP to BCO is also fast. The formed CHE is mainly hydrogenated to CHN due to the high hydrogenation activity of Ru/α-Al_2O_3, which results in the extremely low yield of BCO. The formation of BCO from CPE through the intramolecular rearrangement is another pathway but its degree is significantly lower than the alkylation reaction as reported in the literature [71], especially for the catalyst with high activity. Therefore, Ru/α-Al_2O_3 catalyst tends to catalyze the hydrogenation of aromatic ring.

3.5. Scope of substrates

With the optimized catalyst in hand, the scope of different aromatic substrates was investigated, as listed in Table 7. A 100% conversion can be achieved under mild conditions for all the cases. All the substrates with a single aromatic ring can be hydrogenated to the target product with a yield of 100% (entries 1–12) except for benzoic acid (only a yield of 95.5%, entry 13). When compared with the reported result for the hydrogenation of both BEN and PHE under a high temperature and a high H_2 pressure, the present study achieves a complete conversion and a 100% yield of the products under extremely mild conditions (30 °C and 1 MPa H_2) (Fig. 6d and Table S1, S2). It is noteworthy that the aromatics without oxygen atoms including BEN, toluene, xylene, biphenyl and naphthalene are present in the crude oil with unsaturated hydrocarbons. It is reported by other works that the hydrogenation reaction is a critical process to improve the quality of the crude oil by converting the unsaturated hydrocarbons to the saturated hydrocarbons [42,74]. These previous works show that these hydrogenation reactions need to be performed under a relatively high temperature and a relatively high H_2 pressure, especially for the compounds of naphthalene or biphenyl, which are highly difficult to be completely hydrogenated. Biphenyl is reported to be completely hydrogenated under a relatively high temperature of 250 °C with a Ru-based catalyst [75]. In contrast, the hydrogenation reactions in the present work can occur smoothly over Ru/α-Al_2O_3 at room temperature, even with naphthalene or biphenyl as the substrates (entries 18–19).

In addition, it is beneficial for the fine chemical industry but is challenging if some oxygen-contained functional groups in lignin-derived compounds can be maintained after the hydrogenation of aromatic ring. For the entries of 6–9 and 13, lignin-derived aromatics with hydroxyl, carboxyl or ester groups are converted to the aliphatic chemicals successfully with a yield of 95.5–100%. In contrast, other studies show that the hydrogenation with aprotic organic solvents is negligible over the Ru- and Pd-based catalysts at room temperature [36,61]. The carboxyl group can be maintained after the reaction of benzoic acid because the polar solvent, such as isopropanol, causes the carboxyl group to face the solvent while the aromatic ring to face the catalyst, which leads to the desired hydrogenation of aromatic ring. The result in Fig. S6 calculated by the Fukui function [76,77] also indicates that the hydrogenation of aromatic ring of benzoic acid takes precedence over the reduction of carboxyl group. Moreover, other studies suggest that the hydrogenation of aromatic ring tends to occur rather than the reduction of functional groups under mild conditions [78,79]. The hydrogenation reaction converts the substrates with two phenyl rings to the saturated-ring products with a relatively high yield under mild conditions (entries 14–17). In addition, the cleavage of the C-O bond hardly occurs even for the substrates of benzyl ether (entries 15 and 17). The performance in the selective hydrogenation of aromatic ring over Ru/α-Al_2O_3 catalyst is excellent for the aromatics of phenols, ethers and lipids but is extremely low for the substrates of nitrobenzene, chlorobenzene and other compounds with severe deactivation of aromatic ring. Therefore, the future work is to adjust the structure of the catalyst to achieve the selective hydrogenation of these stable compounds.

4. Conclusions

The performance of Ru/α-Al_2O_3 in the selective hydrogenation of aromatic ring of different lignin-derived compounds at room temperature by using H_2 as the only source of hydrogen is excellent and is better than other types of Ru- and Pd-based catalysts tested. A unique and strong metal-support interaction for Ru/γ-Al_2O_3 indicates that the Ru species are positive-charged due to the existence of the interfacial bonding of Ru-O-Al, which leads to the relatively low activity of Ru/γ-Al_2O_3. No activity can be found for Pd/α-Al_2O_3 with a relatively large particle size of Pd. When compared with other Ru- and Pd-based catalysts tested in the present study, the higher content of metal Ru in Ru/α-Al_2O_3 detected with XPS and XAS facilitates the fast dissociation of H_2 to form the active hydrogen radicals. The DFT calculation shows that Ru/α-Al_2O_3 has a higher adsorption energy of DPE for the hydrogenation of aromatic ring. Furthermore, the selective hydrogenation of aromatic hydrocarbons with specific functional groups to the corresponding aliphatic compounds can be also achieved over Ru/α-Al_2O_3. Therefore, the application of Ru/α-Al_2O_3 catalyst is promising to accelerate the production of sustainable platform chemicals.

CRediT authorship contribution statement

Wei Jiang: Methodology, Conceptualization, Software, Investigation, Formal analysis, Visualization, Writing – original draft preparation. **Jing-Pei Cao:** Conceptualization, Supervision, Writing – review & editing, Funding acquisition, Project administration. **Chen Zhu:** Visualization, Software, Writing – original draft preparation. **Ming Zhao:** Visualization, Software, Writing – original draft preparation. **Zhong-Hai Ni:** Visualization, Software, Writing – original draft preparation. **Xiao-Yan Zhao:** Discussion, Writing – original draft preparation, Writing – review & editing. **Jin-Xuan Xie:** Investigation, Formal analysis. **Liang Zhao:** Investigation, Formal analysis. **Yun-Peng Zhao:** Software, Validation, Formal analysis, Visualization. **Hong-Cun Bai:** Software, Validation, Formal analysis, Visualization.

Declaration of Competing Interest

The authors declare that they have no known competing financial interests or personal relationships that could have appeared to influence the work reported in this paper.

Acknowledgements

This work was supported by the National Key Research and Development Program of China (Grant 2017YFE0124200), the National Natural Science Foundation of China (Grants 21978317), the Natural Science Foundation of Jiangsu Province (Grant BK20200028), the Fundamental Research Funds for the Central Universities (2021YCPY0201) and the Priority Academic Program Development of Jiangsu Higher Education Institutions.

Appendix A. Supporting information

Supplementary data associated with this article can be found in the online version at doi:10.1016/j.apcatb.2022.121137.

References

[1] C.E.J.J. Vriamont, T. Chen, C. Romain, P. Corbett, P. Manageracharath, J. Peet, C. M. Conifer, J.P. Hallett, G.J.P. Britovsek, From lignin to chemicals: hydrogenation of lignin models and mechanistic insights into hydrodeoxygenation via low-temperature C-O bond cleavage, ACS Catal. 9 (2019) 2345–2354.

[2] C.O. Tuck, E. Pérez, I.T. Horváth, R.A. Sheldon, M. Poliakoff, Valorization of biomass: deriving more value from waste, Science 337 (2012) 695–699.
[3] F. Gao, J.D. Webb, J.F. Hartwig, Chemo- and regioselective hydrogenolysis of diaryl ether C-O bonds by a robust heterogeneous Ni/C catalyst: applications to the cleavage of complex lignin-related rragments, Angew. Chem. Int. Ed. 55 (2016) 1474–1478.
[4] A.W. Bartling, M.L. Stone, R.J. Hanes, A. Bhatt, Y.M. Zhang, M.J. Biddy, R. Davis, J.S. Kruger, N.E. Thornburg, J.S. Luterbacher, R. Rinaldi, J.S.M. Samec, B.F. Sels, Y. Román-Leshkov, G.T. Beckham, Techno-economic analysis and life cycle assessment of a biorefinery utilizing reductive catalytic fractionation, Energy Environ. Sci. 14 (2021) 4147–4168.
[5] M.M. Abu-Omar, K. Barta, G.T. Beckham, J.S. Luterbacher, J. Ralph, R. Rinaldi, Y. Román-Leshkov, J.S.M. Samec, B.F. Sels, F. Wang, Guidelines for performing lignin-first biorefining, Energy Environ. Sci. 14 (2021) 262–292.
[6] Q.L. Meng, J. Yan, R.Z. Wu, H.Z. Liu, Y. Sun, N.N. Wu, J.F. Xiang, L.R. Zheng, J. Zhang, B.X. Han, Sustainable production of benzene from lignin, Nat. Commun. 12 (2021) 4534.
[7] M. Guo, J. Peng, Q.H. Yang, C. Li, Highly active and selective RuPd bimetallic NPs for the cleavage of the diphenyl ether C-O bond, ACS Catal. 8 (2018) 11174–11183.
[8] S.H. Zhu, H. Liu, S. Wang, X.Q. Gao, P.F. Wang, J.G. Wang, W.B. Fan, One-step efficient non-hydrogen conversion of cellulose into γ-valerolactone over AgPW/CoNi@NG composite, Appl. Catal. B Environ. 284 (2021), 119698.
[9] C.Z. Li, X.C. Zhao, A.Q. Wang, G.W. Huber, T. Zhang, Catalytic transformation of lignin for the production of chemicals and fuels, Chem. Rev. 115 (2015) 11559–11624.
[10] X.J. Cui, A.E. Surkus, K. Junge, C. Topf, J. Radnik, C. Kreyenschulte, M. Beller, Highly selective hydrogenation of arenes using nanostructured ruthenium catalysts modified with a carbon-nitrogen matrix, Nat. Commun. 7 (2016) 11326.
[11] S.K. Hanson, R.T. Baker, Knocking on wood: base metal complexes as catalysts for selective oxidation of lignin models and extracts, Acc. Chem. Res. 48 (2015) 2037–2048.
[12] V. Stavila, R. Parthasarathi, R.W. Davis, F. El Gabaly, K.L. Sale, B.A. Simmons, S. Singh, M.D. Allendorf, MOF-based catalysts for selective hydrogenolysis of carbon-oxygen ether bonds, ACS Catal. 6 (2016) 55–59.
[13] C.B. Cheng, D.K. Shen, S. Gu, K.H. Luo, State-of-the-art catalytic hydrogenolysis of lignin for the production of aromatic chemicals, Catal. Sci. Technol. 8 (2018) 6275–6296.
[14] M. Zaheer, R. Kempe, Catalytic hydrogenolysis of aryl ethers: a key step in lignin valorization to valuable chemicals, ACS Catal. 5 (2015) 1675–1684.
[15] J.G. Zhang, H. Asakura, J. van Rijn, J. Yang, P. Duchesne, B. Zhang, X. Chen, P. Zhang, M. Saeys, N. Yan, Highly efficient, NiAu-catalyzed hydrogenolysis of lignin into phenolic chemicals, Green Chem. 16 (2014) 2432–2437.
[16] M. Chatterjee, A. Chatterjee, T. Ishizaka, H. Kawanami, Rhodium-mediated hydrogenolysis/hydrolysis of the aryl ether bond in supercritical carbon dioxide/water: an experimental and theoretical approach, Catal. Sci. Technol. 5 (2015) 1532–1539.
[17] L. Dong, Y. Xin, X.H. Liu, Y. Guo, C.W. Pao, J.L. Chen, Y.Q. Wang, Selective hydrodeoxygenation of lignin oil to valuable phenolics over Au/Nb_2O_5 in water, Green Chem. 21 (2019) 3081–3090.
[18] X.M. Dou, W.Z. Li, C.F. Zhu, X. Jiang, Catalytic waste Kraft lignin hydrodeoxygenation to liquid fuels over a hollow Ni-Fe catalyst, Appl. Catal. B Environ. 287 (2021), 119975.
[19] L. Jiang, H.W. Guo, C.Z. Li, P. Zhou, Z.H. Zhang, Selective cleavage of lignin and lignin model compounds without external hydrogen, catalyzed by heterogeneous nickel catalysts, Chem. Sci. 10 (2019) 4458–4468.
[20] Y. Song, Z. Li, P.F. Ji, M. Kaufmann, X.Y. Feng, J.S. Chen, C. Wang, W.B. Lin, Metal-organic framework nodes support single-site nickel(II) hydride catalysts for the hydrogenolysis of aryl ethers, ACS Catal. 9 (2019) 1578–1583.
[21] C. Zhu, J.P. Cao, X.Y. Zhao, T. Xie, J. Ren, X.Y. Wei, Mechanism of Ni-catalyzed selective C-O cleavage of lignin model compound benzyl phenyl ether under mild conditions, J. Energy Inst. 92 (2019) 74–81.
[22] M. Wang, H. Shi, D.M. Camaioni, J.A. Lercher, Palladium-catalyzed hydrolytic cleavage of aromatic C-O bonds, Angew. Chem. Int. Ed. 56 (2017) 2110–2114.
[23] H.R. Wu, Jl Song, C. Xie, C.Y. Wu, C.J. Chen, B.X. Han, Efficient and mild transfer hydrogenolytic cleavage of aromatic ether bonds in lignin-derived compounds over Ru/C, ACS Sustain. Chem. Eng. 6 (2018) 2872–2877.
[24] L. Wang, J. Zhang, X.F. Yi, A.M. Zheng, F. Deng, C.Y. Chen, Y.Y. Ji, F.J. Liu, X. J. Meng, F.S. Xiao, Mesoporous ZSM-5 zeolite-supported Ru nanoparticles as highly efficient catalysts for upgrading phenolic biomolecules, ACS Catal. 5 (2015) 2727–2734.
[25] S.X. Bai, L.Z. Bu, Q. Shao, X. Zhu, X.Q. Huang, Multicomponent Pt-based zigzag nanowires as selectivity controllers for selective hydrogenation reactions, J. Am. Chem. Soc. 140 (2018) 8384–8387.
[26] H. Miyamura, A. Suzuki, T. Yasukawa, S. Kobayashi, Polysilane-immobilized Rh-Pt bimetallic nanoparticles as powerful arene hydrogenation catalysts: synthesis, reactions under batch and flow conditions and reaction mechanism, J. Am. Chem. Soc. 140 (2018) 11325–11334.
[27] P. Das, P.P. Sarmah, B.J. Borah, L. Saikia, D.K. Dutta, Aromatic ring hydrogenation catalysed by nanoporous montmorillonite supported Ir(0)-nanoparticle composites under solvent free conditions, New J. Chem. 40 (2016) 2850–2855.
[28] D. Moock, M.P. Wiesenfeldt, M. Freitag, S. Muratsugu, S. Ikemoto, R. Knitsch, J. Schneidewind, W. Baumann, A.H. Schafer, A. Timmer, M. Tada, M.R. Hansen, F. Glorius, Mechanistic understanding of the heterogeneous, rhodium-cyclic (alkyl)(amino)carbene-catalyzed (fluoro-)arene hydrogenation, ACS Catal. 10 (2020) 6309–6317.
[29] A.G. Sergeev, J.D. Webb, J.F. Hartwig, A heterogeneous nickel catalyst for the hydrogenolysis of aryl ethers without arene hydrogenation, J. Am. Chem. Soc. 134 (2012) 20226–20229.
[30] V. Molinari, C. Giordano, M. Antonietti, D. Esposito, Titanium nitride-nickel nanocomposite as heterogeneous catalyst for the hydrogenolysis of aryl ethers, J. Am. Chem. Soc. 136 (2014) 1758–1761.
[31] X.H. Liu, L.J. Xu, G.Y. Xu, W.D. Jia, Y.F. Ma, Y. Zhang, Selective hydrodeoxygenation of lignin-derived phenols to cyclohexanols or cyclohexanes over magnetic CoNx@NC catalysts under mild conditions, ACS Catal. 6 (2016) 7611–7620.
[32] G. Pieters, C. Taglang, E. Bonnefille, T. Gutmann, C. Puente, J.C. Berthet, C. Dugave, B. Chaudret, B. Rousseau, Regioselective and stereospecific deuteration of bioactive aza compounds by the use of ruthenium nanoparticles, Angew. Chem. Int. Ed. 53 (2014) 230–234.
[33] B.F. Machado, M. Oubenali, M. Rosa Axet, T. Trang Nguyen, M. Tunckol, M. Girleanu, O. Ersen, I.C. Gerber, P. Serp, Understanding the surface chemistry of carbon nanotubes: toward a rational design of Ru nanocatalysts, J. Catal. 309 (2014) 185–198.
[34] Y. Wang, J. Yao, H.R. Li, D.S. Su, M. Antonietti, Highly selective hydrogenation of phenol and derivatives over a Pd@carbon nitride catalyst in aqueous media, J. Am. Chem. Soc. 133 (2011) 2362–2365.
[35] R. Raja, T. Khimyak, J.M. Thomas, S. Hermans, B.F.G. Johnson, Single-step, highly active, and highly selective nanoparticle catalysts for the hydrogenation of key organic compounds, Angew. Chem. Int. Ed. 40 (2001) 4638–4642.
[36] X.M. Ren, M. Guo, H. Li, C.B. Li, L. Yu, J. Liu, Q.H. Yang, Microenvironment engineering of ruthenium nanoparticles incorporated into silica nanoreactors for enhanced hydrogenations, Angew. Chem. Int. Ed. 58 (2019) 14483–14488.
[37] L.C. Liu, A. Corma, Metal catalysts for heterogeneous catalysis: from single atoms to nanoclusters and nanoparticles, Chem. Rev. 118 (2018) 4981–5079.
[38] V. Vinokurov, A. Glotov, Y. Chudakov, A. Stavitskaya, E. Ivanov, P. Gushchin, A. Zolotukhina, A. Maximov, E. Karakhanov, Y. Lvov, Core/shell ruthenium-halloysite nanocatalysts for hydrogenation of phenol, Ind. Eng. Chem. Res. 56 (2017) 14043–14052.
[39] Y. Li, G.J. Lan, H.Y. Wang, H.D. Tang, X.H. Yan, H.Z. Liu, Controlled synthesis of highly dispersed semi-embedded ruthenium nanoparticles in porous carbon framework with more exposed active sites, Catal. Commun. 20 (2012) 29–35.
[40] A. Maximov, A. Zolotukhina, V. Murzin, E. Karakhanov, E. Rosenberg, Ruthenium nanoparticles stabilized in cross-linked dendrimer matrices: hydrogenation of phenols in aqueous media, ChemCatChem 7 (2015) 1197–1210.
[41] M.L. Hua, J.L. Song, C. Xie, H.R. Wu, Y. Hu, X. Huang, B.X. Han, Ru/hydroxyapatite as a dual-functional catalyst for efficient transfer hydrogenolytic cleavage of aromatic ether bonds without additional bases, Green Chem. 21 (2019) 5073–5079.
[42] X.C. Kang, J.L. Zhang, W.T. Shang, T.B. Wu, P. Zhang, B.X. Han, Z.H. Wu, G. Mo, X. Q. Xing, One-step synthesis of highly efficient nanocatalysts on the supports with hierarchical pores using porous ionic liquid-water gel, J. Am. Chem. Soc. 136 (2014) 3768–3771.
[43] A.N. Raut, S.U. Nandanwar, Y.R. Suryawanshi, M. Chakraborty, S. Jauhari, S. Mukhopadhyay, K.T. Shenoy, H.C. Bajaj, Liquid phase selective hydrogenation of phenol to cyclohexanone over Ru/Al_2O_3 nanocatalyst under mild conditions, Kinet. Catal. 57 (2016) 39–46.
[44] K. Morawa Eblagon, K. Tam, K.M.K. Yu, S.L. Zhao, X.Q. Gong, H.Y. He, L. Ye, L. C. Wang, A.J. Ramirez-Cuesta, S.C. Tsang, Study of catalytic sites on ruthenium for hydrogenation of *N*-ethylcarbazole: Implications of hydrogen storage via reversible catalytic hydrogenation, J. Phys. Chem. C 114 (2010) 9720–9730.
[45] K.C. Tan, T. He, Y.S. Chua, P. Chen, Recent advances of catalysis in the hydrogenation and dehydrogenation of N-heterocycles for hydrogen storage, J. Phys. Chem. C 125 (2021) 18553–18566.
[46] S. Furukawa, Y. Matsunami, I. Hamada, Y. Hashimoto, Y. Sato, T. Komatsu, Remarkable enhancement in hydrogenation ability by phosphidation of ruthenium: specific surface structure having unique Ru ensembles, ACS Catal. 8 (2018) 8177–8181.
[47] K.H. Park, K. Jang, H.J. Kim, S.U. Son, Near-monodisperse tetrahedral rhodium nanoparticles on charcoal: the shape-dependent catalytic hydrogenation of arenes, Angew. Chem. Int. Ed. 46 (2007) 1152–1155.
[48] E. Bayram, J.C. Linehan, J.L. Fulton, J.A. Roberts, N.K. Szymczak, T. D. Smurthwaite, S. Ozkar, M. Balasubramanian, R.G. Finke, Is it homogeneous or heterogeneous catalysis derived from $[RhCp^*Cl_2]_2$? In operando XAFS, kinetic, and crucial kinetic poisoning evidence for subnanometer Rh_4 cluster-based benzene hydrogenation catalysis, J. Am. Chem. Soc. 133 (2011) 18889–18902.
[49] C. Hubert, A. Denicourt-Nowicki, P. Beaunier, A. Roucoux, TiO_2-supported Rh nanoparticles: from green catalyst preparation to application in arene hydrogenation in neat water, Green Chem. 12 (2010) 1167–1170.
[50] A. Miyazaki, I. Balint, K. Aika, Y. Nakano, Preparation of Ru nanoparticles supported on γ-Al_2O_3 and its novel catalytic activity for ammonia synthesis, J. Catal. 204 (2001) 364–371.
[51] C. Milone, G. Neri, A. Donato, M.G. Musolino, L. Mercadante, Selective hydrogenation of benzene to cyclohexene on Ru/γ-Al_2O_3, J. Catal. 159 (1996) 253–258.
[52] X.R. Chen, H.B. Zou, S.Z. Chen, X.F. Dong, W.M. Lin, Selective oxidation of CO in excess H_2 over Ru/Al_2O_3 catalysts modified with metal oxide, J. Nat. Gas Chem. 16 (2007) 409–414.
[53] A. Berman, R.K. Karn, M. Epstein, Kinetics of steam reforming of methane on Ru/Al_2O_3 catalyst promoted with Mn oxides, Appl. Catal. A Gen. 282 (2005) 73–83.

[54] C. Zhu, J.P. Cao, X.Y. Zhao, T. Xie, M. Zhao, X.Y. Wei, Bimetallic effects in the catalytic hydrogenolysis of lignin and its model compounds on Nickel-Ruthenium catalysts, Fuel Process. Technol. 194 (2019), 106126.
[55] T.N. Phan, Y.K. Park, I.G. Lee, C.H. Ko, Enhancement of C-O bond cleavage to afford aromatics in the hydrodeoxygenation of anisole over ruthenium-supporting mesoporous metal oxides, Appl. Catal. A Gen. 544 (2017) 84–93.
[56] T. Xie, J.P. Cao, C. Zhu, X.Y. Zhao, M. Zhao, Y.P. Zhao, X.Y. Wei, Selective cleavage of C-O bond in benzyl phenyl ether over Pd/AC at room temperature, Fuel Process. Technol. 188 (2019) 190–196.
[57] J. Yi, Y.P. Luo, T. He, Z.C. Jiang, J.M. Li, C.W. Hu, High efficient hydrogenation of lignin-derived monophenols to cyclohexanols over Pd/γ-Al_2O_3 under mild conditions, Catalysts 6 (2016) 12.
[58] J. Dupont, J.D. Scholten, On the structural and surface properties of transition-metal nanoparticles in ionic liquids, Chem. Soc. Rev. 39 (2010) 1780–1804.
[59] L. Chen, J.Y. Xin, L.L. Ni, H.X. Dong, D.X. Yan, X.M. Lu, S.J. Zhang, Conversion of lignin model compounds under mild conditions in pseudo-homogeneous systems, Green Chem. 18 (2016) 2341–2352.
[60] J.A. Anderson, F.M. McKenna, A. Linares-Solano, R.P.K. Wells, Use of water as a solvent in directing hydrogenation reactions of aromatic acids over Pd-carbon nanofibre catalysts, Catal. Lett. 119 (2007) 16–20.
[61] X. Xu, M.H. Tang, M.M. Li, H.R. Li, Y. Wang, Hydrogenation of benzoic acid and derivatives over Pd nanoparticles supported on N-doped carbon derived from glucosamine hydrochloride, ACS Catal. 4 (2014) 3132–3135.
[62] S.Z. Wang, K.L. Zhang, H.L. Li, L.P. Xiao, G.Y. Song, Selective hydrogenolysis of catechyl lignin into propenylcatechol over an atomically dispersed ruthenium catalyst, Nat. Commun. 12 (2021) 416.
[63] M.L. Xiao, L.Q. Gao, Y. Wang, X. Wang, J.B. Zhu, Z. Jin, C.P. Liu, H.Q. Chen, G. R. Li, J.J. Ge, Q.G. He, Z.J. Wu, Z.W. Chen, W. Xing, Engineering energy level of metal center: Ru single-atom site for efficient and durable oxygen reduction catalysis, J. Am. Chem. Soc. 141 (2019) 19800–19806.
[64] J.J. Mao, C.T. He, J.J. Pei, W.X. Chen, D.S. He, Y.Q. He, Z.B. Zhuang, C. Chen, Q. Peng, D.S. Wang, Y.D. Li, Accelerating water dissociation kinetics by isolating cobalt atoms into ruthenium lattice, Nat. Commun. 9 (2018) 4958.
[65] S.F. Chen, J.L. Li, Y.H. Zhang, Y.X. Zhao, K.Y. Liew, J.P. Hong, Production of lower olefins with highly dispersed Ru catalysts supported on Al-SBA-15 in Fischer-Tropsch synthesis, Top. Catal. 57 (2014) 437–444.
[66] M. Machida, Y. Uchida, Y. Ishikawa, S. Hinokuma, H. Yoshida, J. Ohyama, Y. Nagao, Y. Endo, K. Iwashina, Y. Nakahara, Thermostable Rh metal nanoparticles formed on Al_2O_3 by high-temperature H_2 reduction and its impact on three-way catalysis, J. Phys. Chem. C 123 (2019) 24584–24591.
[67] X.Y. Wang, R. Rinaldi, Solvent effects on the hydrogenolysis of diphenyl ether with Raney nickel and their implications for the conversion of lignin, ChemSusChem 5 (2012) 1455–1466.
[68] U.K. Singh, M.A. Vannice, Kinetics of liquid-phase hydrogenation reactions over supported metal catalysts - a review, Appl. Catal. A Gen. 213 (2001) 1–24.
[69] E. Paone, C. Espro, R. Pietropaolo, F. Mauriello, Selective arene production from transfer hydrogenolysis of benzyl phenyl ether promoted by a co-precipitated Pd/Fe_3O_4 catalyst, Catal. Sci. Technol. 6 (2016) 7937–7941.
[70] B.L. Tran, J.L. Fulton, J.C. Linehan, J.A. Lercher, R.M. Bullock, Rh(CAAC)-catalyzed arene hydrogenation: evidence for nanocatalysis and sterically controlled site-selective hydrogenation, ACS Catal. 8 (2018) 8441–8449.
[71] C.A. Scaldaferri, P. Warakunwit, V.M.D. Pasa, D.E. Resasco, C-O cleavage of diphenyl ether followed by C-C coupling reactions over hydrophobized Pd/HY catalysts, Appl. Catal. B Environ. 259 (2019), 118081.
[72] S.H. Jin, Z.H. Xiao, X. Chen, L. Wang, J. Guo, M. Zhang, C.H. Liang, Cleavage of lignin-derived 4-O-5 aryl ethers over nickel nanoparticles supported on niobic acid-activated carbon composites, Ind. Eng. Chem. Res. 54 (2015) 2302–2310.
[73] F. Mauriello, E. Paone, R. Pietropaolo, A.M. Balu, R. Luque, Catalytic transfer hydrogenolysis of lignin-derived aromatic ethers promoted by bimetallic Pd/Ni systems, ACS Sustain. Chem. Eng. 6 (2018) 9269–9276.
[74] S. Akbayrak, Rhodium(0) nanoparticles supported on ceria as catalysts in hydrogenation of neat benzene at room temperature, J. Colloid Interface Sci. 530 (2018) 459–464.
[75] H.L. Wang, H.M. Wang, E. Kuhn, M.P. Tucker, B. Yang, Production of jet fuel-range hydrocarbons from hydrodeoxygenation of lignin over super lewis acid combined with metal catalysts, ChemSusChem 11 (2018) 285–291.
[76] Y. Li, J.N.S. Evans, The Fukui function: a key concept linking frontier molecular orbital theory and the hard-soft-acid-base principle, J. Am. Chem. Soc. 117 (1995) 7756–7759.
[77] T.C. Allison, T.Y.Y. J, Application of the condensed Fukui function to predict reactivity in core-shell transition metal nanoparticles, Electrochim. Acta 101 (2013) 334–340.
[78] R.F. Nie, H.Z. Jiang, X.H. Lu, D. Zhou, Q.H. Xia, Highly active electron-deficient Pd clusters on N-doped active carbon for aromatic ring hydrogenation, Catal. Sci. Technol. 6 (2016) 1913–1920.
[79] M.H. Tang, S.J. Mao, M.M. Li, Z.Z. Wei, F. Xu, H.R. Li, Y. Wang, RuPd alloy nanoparticles supported on N-doped carbon as an efficient and stable catalyst for benzoic acid hydrogenation, ACS Catal. 5 (2015) 3100–3107.